Lee *et al. Nano Convergence* (2026) 13:46
https://doi.org/10.1186/s40580-026-00580-y

Nano Convergence

FULL PAPER Open Access

Amplification-free colorimetric detection of exosomal miRNA using a CRISPR/Cas13a-activated HRP/Au/MoS_2 nanobiohybrid catalyst

Myeong-Jun Lee[1†], Minkyu Shin[2†], Joungpyo Lim[1], Ha Rim Ahn[3], Dain Jung[1], Shan Liu[4], Chenzhong Li[5], Jin-Ha Choi[6*] and Jeong-Woo Choi[1*]

Abstract

CRISPR-based, amplification-free colorimetric sensing has emerged as a powerful approach for exosomal miRNA (Exo-miR) analysis, offering high specificity, simple operation, and direct visual readout suitable for point-of-care diagnostics. However, the sensitivity of existing systems is limited because conventional colorimetric probes generate inherently weak signals, making the reliable detection of ultralow-abundance Exo-miRs difficult without amplification. Here, we firstly report an amplification-free colorimetric biosensor based on a horseradish peroxidase (HRP)/gold nanoparticle (Au)/molybdenum disulfide (MoS_2) nanobiohybrid catalyst (HRP/Au/MoS_2) that generates intense chromogenic signals via synergistic catalytic interactions. In this nanoparticle, MoS_2 provides a high-surface-area scaffold with intrinsic peroxidase-like activity, Au nanoparticles facilitate efficient electron transfer, and HRP contributes to high catalytic turnover. Together, these features markedly enhance the oxidation of 3,3′,5,5′-tetramethylbenzidine (TMB) and the resulting blue coloration. Using this signal-amplifying HRP/Au/MoS_2, a magnet-based sensing system was constructed by immobilizing the HRP/Au/MoS_2 onto magnetic nanobeads (MNBs) through biotinylated single-stranded RNA linkers (MNB–ssRNA–HRP/Au/MoS_2). This construction was then integrated into a CRISPR/Cas13a assay, in which the target miR-155 activates Cas13a, which cleaves the ssRNA linkers, releasing the HRP/Au/MoS_2 into solution for colorimetric readout. The resulting biosensor exhibits a detection range of 1 fM–1 nM (LOD = 0.82 fM), and single-nucleotide specificity without nucleic acid amplification. Furthermore, our system enables detection of Exo-miR-155 in both cell-derived exosomes and clinical samples, distinguishing cancer patients from healthy donors. Therefore, this platform represents a promising approach for highly sensitive, selective, simple, and time-efficient detection of Exo-miR, which can be used for liquid biopsy-based early cancer detection.

[†]Myeong-Jun Lee and Minkyu Shin contributed equally to this work.

*Correspondence:
Jin-Ha Choi
jhchoi@jbnu.ac.kr
Jeong-Woo Choi
jwchoi@sogang.ac.kr

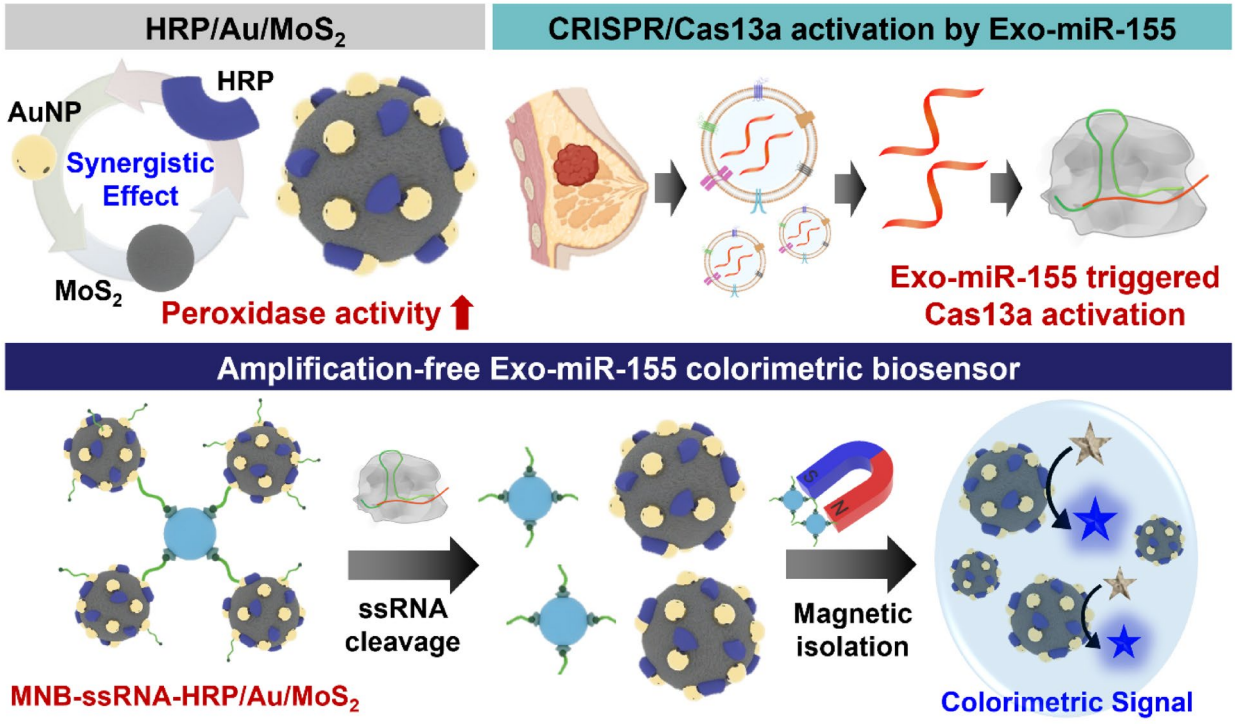
Full list of author information is available at the end of the article

© The Author(s) 2026. **Open Access** This article is licensed under a Creative Commons Attribution-NonCommercial-NoDerivatives 4.0 International License, which permits any non-commercial use, sharing, distribution and reproduction in any medium or format, as long as you give appropriate credit to the original author(s) and the source, provide a link to the Creative Commons licence, and indicate if you modified the licensed material. You do not have permission under this licence to share adapted material derived from this article or parts of it. The images or other third party material in this article are included in the article's Creative Commons licence, unless indicated otherwise in a credit line to the material. If material is not included in the article's Creative Commons licence and your intended use is not permitted by statutory regulation or exceeds the permitted use, you will need to obtain permission directly from the copyright holder. To view a copy of this licence, visit http://creativecommons.org/licenses/by-nc-nd/4.0/.

Springer

Keywords Nanobiohybrid catalyst, Exosomal miRNA, Colorimetric biosensor, CRISPR/Cas13a, Breast cancer

Graphical abstract



1 Introduction

Exosomal microRNAs (Exo-miRs) have emerged as highly valuable biomarkers for disease diagnosis and monitoring because these miRNAs mediate post-transcriptional gene regulation and reflect the physiological state of the associated cells of origin [1–3]. Encapsulated within the protective lipid bilayer of exosomes, these miRs remain stable during circulation in body fluids such as blood, urine, and saliva, making the encapsulated miRs accessible through minimally invasive sampling [4, 5]. Numerous studies have demonstrated that specific Exo-miRs signatures correlate strongly with pathological conditions, including cancer, cardiovascular disease, and neurological disorders. For instance, elevated levels of miR-21, miR-155, and miR-423-5p have been observed in breast cancer (B.C.) and are associated with disease progression [6–8]. These findings underscore the diagnostic potential of Exo-miRs and highlight the growing need for technologies capable of accurately and rapidly detecting these encapsulated miRs.

Despite the associated clinical relevance, direct detection of Exo-miRs remains extremely challenging because of the remarkably low natural abundance of Exo-miRs [9, 10]. Even in disease states, Exo-miR levels typically fall within the femtomolar to picomolar range, far below the detection limits of most conventional analytical methods [11]. This low concentration is further compounded by the intrinsic complexity of biological fluids, in which structurally similar nucleic acids and protein contaminants can interfere with accurate detection. Therefore, highly sensitive and selective analytical platforms are essential for reliably quantifying Exo-miRs without extensive sample processing or pre-amplification steps [12]. Indeed, overcoming this fundamental analytical barrier is crucial for translating Exo-miR biomarkers into practical diagnostic tools suitable for early disease detection and clinical decision-making.

Recently, clustered regularly interspaced short palindromic repeats (CRISPR)-based molecular diagnostics have emerged as a powerful solution to the sensitivity and specificity limitations of traditional nucleic acid detection methods [13]. In particular, CRISPR/Cas13a has attracted considerable attention because of the associated programmable RNA-guided recognition and collateral cleavage of single-stranded RNA (ssRNA) [14]. Upon target miR binding, Cas13a is activated and initiates *trans*-cleavage of nearby RNA sequences, enabling sensitive detection without requiring complex amplification steps. CRISPR systems such as SHERLOCK have demonstrated single-nucleotide discrimination and

robust analytical performance, making these systems highly attractive for miR sensing [15]. However, most CRISPR diagnostic platforms rely on fluorescence or electrochemical readouts, both of which require external instrumentation [16]. Fluorescence assays also necessitate laser sources and detectors, whereas electrochemical analysis requires electrode fabrication and specialized readers, thereby limiting portability and hindering point-of-care implementation.

Therefore, colorimetric detection methods have gained increasing attention as a practical alternative for CRISPR-based biosensing [17]. Colorimetric assays provide rapid, equipment-free, and visually interpretable outputs, making these systems well-suited for point-of-care applications and field deployment. The oxidation of chromogenic substrates such as 3,3′,5,5′-tetramethylbenzidine (TMB) by horseradish peroxidase (HRP) or nanozyme catalysts produces distinct color changes that can be quantified spectroscopically or observed directly with the naked eye [18]. These operational advantages simplify workflows and facilitate broader clinical accessibility. Nevertheless, the intrinsic signal intensity of conventional colorimetric systems is often insufficient to detect extremely low-abundance targets such as Exo-miRs [19]. Without strong catalytic amplification, the color change remains weak or undetectable at low target concentrations, thereby limiting the sensitivity of amplification-free colorimetric platforms.

Thus, achieving high sensitivity in colorimetric CRISPR diagnostics requires the development of catalytic nanomaterials capable of generating significantly stronger chromogenic signals. Nanozymes such as gold nanoparticles (AuNPs), molybdenum disulfide (MoS_2) nanosheets, and graphene derivatives have been investigated for the associated peroxidase-mimicking properties [20–22]. However, many of these materials exhibit only moderate catalytic activity or require extensive surface functionalization, which complicates the integration of these materials with CRISPR systems. Therefore, there remains a critical unmet need for a highly stable and synergistically active nanozyme capable of dramatically enhancing colorimetric signal output, particularly in amplification-free assays targeting Exo-miRs.

To address this challenge, we aimed to develop a highly sensitive, amplification-free Exo-miR colorimetric biosensor comprising an HRP/Au/MoS_2 nanobiohybrid catalyst complex integrated with CRISPR/Cas13a. Moreover, to establish a sensitive amplification-free colorimetric platform, we initially aimed to construct a nanobiohybrid catalyst by integrating HRP, AuNPs, and MoS_2 nanoparticles (NPs) into a single nanoparticle (HRP/Au/MoS_2) architecture with markedly enhanced peroxidase activity (Fig. 1A). MoS_2 provides a high-surface-area platform with inherent peroxidase-like behavior, while AuNPs enhance electron-transfer efficiency and accelerate reaction kinetics [23]. The addition of HRP further amplifies catalytic turnover, creating a powerful multicomponent catalytic interface that drives rapid and intense TMB oxidation. This synergistic nanobiohybrid catalyst design significantly surpasses the catalytic performance of traditional HRP systems or single-component nanoparticles, providing the strong chromogenic output required for sensitive amplification-free detection. Based on this HRP/Au/MoS_2 nanobiohybrid catalyst platform, we constructed a CRISPR/Cas13a biosensor capable of detecting Exo-miRs. Biotinylated ssRNA linkers were conjugated to the HRP/Au/MoS_2 and immobilized on streptavidin-coated magnetic nanobeads (MNB), which were called MNB–ssRNA–HRP/Au/MoS_2 complex (MNB–ssRNA–HRP/Au/MoS_2). Upon recognition of the target Exo-miR-155, a widely used biomarker for BC diagnosis, Cas13a is activated (Fig. 1B). Subsequently, activated CRISPR/Cas13a, in the presence of miR-155, can cleave ssRNA linkers on MNB–ssRNA–HRP/Au/MoS_2, thereby releasing the HRP/Au/MoS_2 into solution (Fig. 1C). The unbound HRP/Au/MoS_2 are then readily separated using magnets. After these washing steps, the released HRP/Au/MoS_2 catalyze the rapid oxidation of TMB, producing a strong blue color proportional to the target Exo-miR-155 concentration. Furthermore, we applied this device to detect miR-155 with high sensitivity and specificity in exosomes derived from various cell lines, thereby confirming the diagnostic significance of this platform for BC. Our findings demonstrate that HRP/Au/MoS_2 nanobiohybrid catalyst-based strong chromogenic signaling combined with the CRISPR/Cas system represents a promising platform for Exo-miR detection that is highly sensitive, selective, simple, and time-efficient.

2 Experimental section

2.1 Materials

Ammonium molybdate tetrahydrate, thiourea, horseradish peroxidase (HRP), hydrogen tetrachloroaurate (III) trihydrate ($HAuCl_4{\cdot}3H_2O$), 1,300 kDa polyvinylpyrrolidone (PVP), hydrocortisone, cholera toxin, and epidermal growth factor (EGF) were purchased from Merck (Germany). Diethylpyrocarbonate (DEPC)-treated nuclease-free water, biotinylated ssRNA, CRISPR guide RNA (crRNA), and target miRNA sequences were obtained from Bioneer (Korea). Streptavidin-modified MNBs (10 mg/mL) were purchased from Bioneer (Korea), and RNase A was obtained from Thermo Fisher Scientific (USA). Tris-borate-EDTA polyacrylamide gels (TBE gels) for electrophoresis were purchased from Bio-Rad (USA). The CRISPR/Cas13a enzyme (LwaCas13a) and reaction buffer were obtained from Genescript (USA). Phosphate-buffered saline (PBS), DMEM/F12 basal medium, RPMI 1640 medium, and penicillin–streptomycin (1%) were

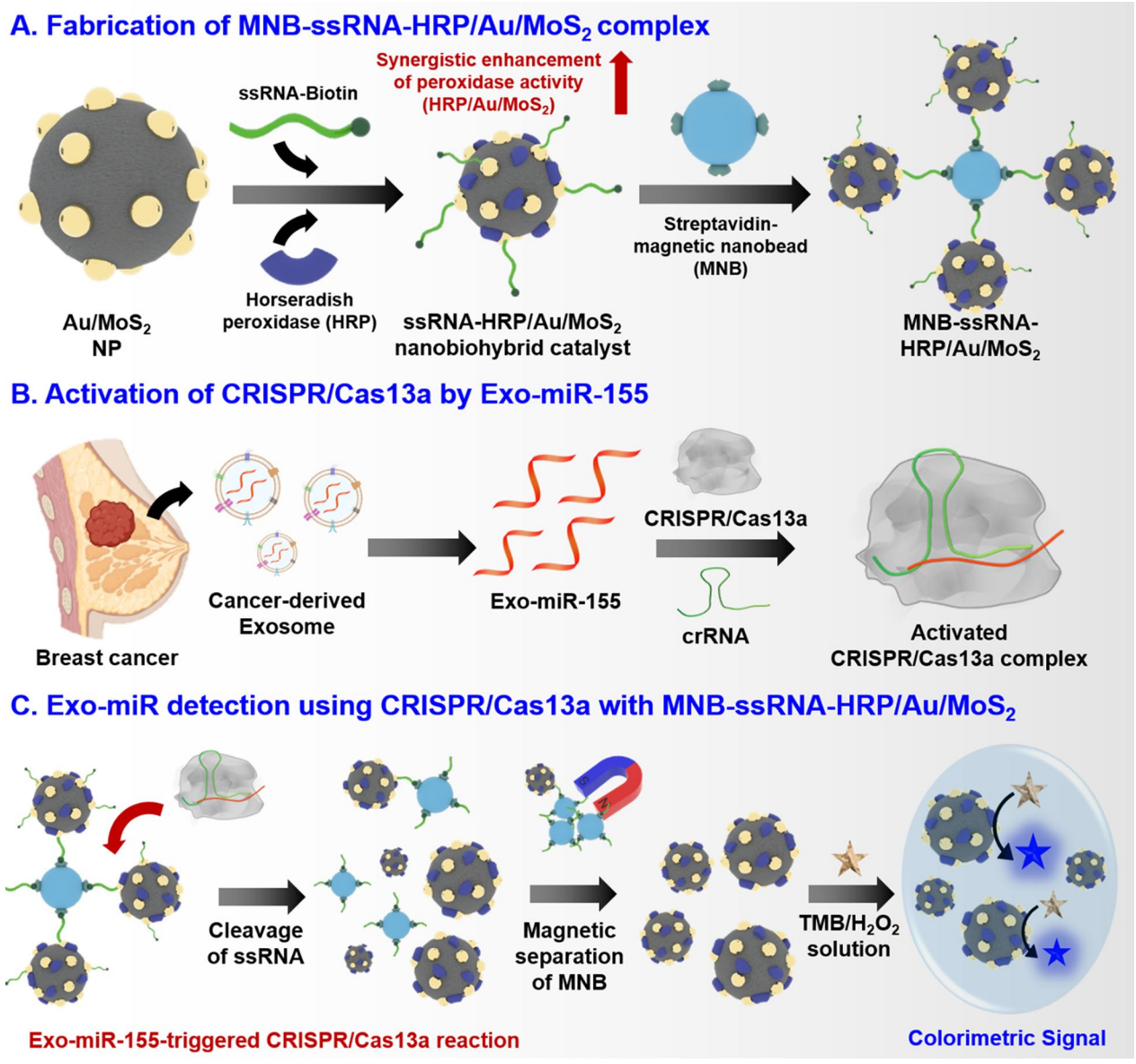


Fig. 1 Schematic illustration of the MNB–ssRNA–HRP/Au/MoS_2-based colorimetric sensing platform. **A** Preparation of the HRP/Au/MoS_2 nanobiohybrid catalyst and assembly of the MNB–ssRNA–HRP/Au/MoS_2 complex via thiolated (5′) and biotinylated (3′) ssRNA linkers. **B** Target recognition mechanism, in which Exo-miR-155 binds to the associated crRNA and activates Cas13a, inducing collateral ssRNA cleavage within the magnetic complex. **C** Cleavage-triggered release of HRP/Au/MoS_2 into solution, enabling strong TMB oxidation and colorimetric signal generation

purchased from Welgene (Korea). Horse serum (HS) and fetal bovine serum (FBS) were obtained from Gibco (USA). The Exo-spin™ exosome isolation kit was purchased from Cell Guidance Systems (UK). Human cell lines, including MCF-10A (non-tumorigenic mammary epithelial cells), MCF-7 (human breast adenocarcinoma cells), and PC-3 (human prostate cancer cells), were obtained from the Korean Cell Line Bank (KCLB, Korea).

2.2 Synthesis of HRP/Au/MoS_2 nanobiohybrid catalyst

To synthesize HRP/Au/MoS_2 nanobiohybrid catalyst, MoS_2 NPs were first prepared. Ammonium molybdate tetrahydrate (0.35 g) and thiourea (0.76 g) were dissolved in 40 mL of deionized (DI) water. Subsequently, 30 k PVP (0.25 g) was added to the prepared solution, and the mixture was stirred at 800 rpm and 60 °C for 1 h. The mixture was transferred to a Teflon-lined stainless-steel autoclave and heated at 200 °C for 24 h. The resulting precipitation was collected and washed with DI water and ethanol by centrifugal filtration at 8,000 rpm for 30 min. To synthesize Au/MoS_2 NPs, 10 mL of the synthesized MoS_2 NPs (1 mg/mL) was mixed with 0.2 g of PVP and stirred at 600 rpm and 25 °C for 90 min. Then, 500 µL of $HAuCl_4$ (100 mM) was added, and the mixture

was further reacted at 600 rpm and 25 °C for 30 min. The resulting solution was washed with DI water and ethanol using centrifugal filtration at 8,000 rpm for 30 min. The final product was stored at 4 °C for several months.

Then, to synthesize HRP/Au/MoS_2, 40 μL of synthesized Au/MoS_2 NPs (1 mg/mL) was mixed with 430 μL of diethyl pyrocarbonate (DEPC)-treated water, 15 μL of HRP (5 mg/mL), and 15 μL of ssRNA (10 μM) and incubated at 4 °C for 24 h. The ssRNA sequence is provided in Table S1. The synthesized HRP/Au/MoS_2 were washed with DEPC-treated water by centrifugal filtration at 8,000 rpm for 15 min. The HRP/Au/MoS_2 were examined using transmission electron microscopy (TEM), dynamic light scattering (DLS), and zeta-potential analyses to confirm successful synthesis. To quantify the amount of HRP immobilized on the Au/MoS_2 surface, the wash supernatant collected after HRP conjugation was analyzed to determine the concentration of unbound HRP. The amount of immobilized HRP was calculated by subtracting the amount of unbound HRP recovered in the wash supernatant from the initially added HRP. The HRP loading efficiency was calculated as the ratio of immobilized HRP to the initially added HRP.

2.3 Enzyme kinetic analysis of HRP/Au/MoS_2

The steady-state kinetic parameters of the HRP/Au/MoS_2 nanobiohybrid catalyst were evaluated using TMB and H_2O_2 as substrates. The catalytic reaction was monitored by measuring the increase in absorbance at 652 nm corresponding to the oxidation of TMB. For the determination of kinetic parameters toward TMB, the concentration of H_2O_2 was fixed at 10 mM, while the final concentration of TMB was varied from 0.05 to 2.0 mM. The reaction mixture consisted of 200 μL of substrate solution prepared in 0.1 M citrate buffer (pH 4.0) and 10 μL of HRP/Au/MoS_2 nanobiohybrid catalyst suspension. Immediately after catalyst addition, the absorbance at 652 nm was continuously recorded using a microplate reader. The initial reaction velocity (v) was determined from the linear region of the absorbance-time curve during 20 s to 60 s of reaction. The initial reaction velocity (v) was calculated from the linear region of the absorbance–time curve (20–60 s) according to Beer–Lambert law:

$$\upsilon = \frac{1}{\varepsilon l} \times \frac{dA}{dt}$$

where ε is the molar extinction coefficient of oxidized TMB (39,000 M^{-1} cm^{-1} at 652 nm) and l is the optical path length of the reaction solution (0.56 cm for 200 μL in a 96-well plate). For the determination of kinetic parameters toward H_2O_2, the concentration of TMB was fixed at 1.0 mM, while the final concentration of H_2O_2 was varied from 0.1 to 50 mM under otherwise identical conditions. The Michaelis–Menten constant (K_m) and maximum reaction velocity (V_{max}) were obtained by fitting the experimental data to the Michaelis–Menten equation using nonlinear regression analysis:

$$\upsilon = \frac{V_{max} \times [S]}{K_m + [S]}$$

where v is the initial reaction velocity and [S] is the substrate concentration. Curve fitting and kinetic parameter calculations were performed using GraphPad Prism 10.

2.4 Preparation of the MNB–ssRNA–HRP/Au/MoS_2 complex

The MNB–ssRNA–HRP/Au/MoS_2 complex was prepared through the interaction between streptavidin and biotin. Specifically, streptavidin-modified MNBs were conjugated to biotinylated ssRNA–HRP/Au/MoS_2. Briefly, 90 μL of MNBs (10 mg/mL), 90 μL of ssRNA–HRP/Au/MoS_2, and 90 μL of DEPC-treated water were mixed at 4 °C for 1 h. The mixed solution was then placed on a neodymium (Nd) magnet for 1 min, after which the supernatant was removed, and 270 μL of DEPC-treated water was added. The step of removing the supernatant and adding DEPC-treated water was repeated three times.

2.5 Confirmation of cleavage of the MNB–ssRNA–HRP/Au/MoS_2 complex

Cleavage of the prepared MNB–ssRNA–HRP/Au/MoS_2 complex was first evaluated using RNase A. Briefly, 20 μL of the MNB–ssRNA–HRP/Au/MoS_2 was mixed with 10 μL of RNase A and incubated at room temperature for 10 min. The reacted MNB–ssRNA–HRP/Au/MoS_2 complex was then placed on an Nd magnet for 1 min, and 20 μL of the supernatant was collected and incubated with 200 μL of TMB solution. The absorbance of the resulting supernatant was measured using a microplate reader. Cleavage of ssRNA by activated CRISPR/Cas13a and RNase A in the MNB–ssRNA–HRP/Au/MoS_2 was further analyzed by Tris–borate–EDTA–polyacrylamide gel electrophoresis (TBE–PAGE).

2.6 Target miRNA detection using the MNB–ssRNA–HRP/Au/MoS_2 complex with CRISPR/Cas13a

For target miRNA detection, a 20 μL CRISPR reaction mixture containing 4 μL of Cas13a protein (1 μM), 4 μL of crRNA (1 μM), 2 μL of 10× CRISPR reaction buffer, 2 μL of target miRNA (final concentrations of 1 nM, 100 pM, 10 pM, 1 pM, 100 fM, 10 fM, or 1 fM), and 8 μL of DEPC-treated water was prepared. The mixture was combined with 20 μL of the pre-synthesized MNB–ssRNA–HRP/Au/MoS_2 complex and incubated at 37 °C for 60 min. After incubation, the reaction solution was placed on an

Nd magnet for 1 min, and 20 μL of the supernatant was collected and transferred to a 96-well plate. Then, 200 μL of TMB substrate solution was added to the isolated supernatant, and the mixture was incubated for 30 min for the colorimetric analysis.

2.7 Cell culture

MCF-10A (non-tumorigenic mammary epithelial cell line) cells were cultured in DMEM/F12 cell culture medium supplemented with 10% horse serum (HS), 1% penicillin–streptomycin antibiotics, 0.5 mg/mL hydrocortisone, 100 ng/mL cholera toxin, and 20 ng/mL EGF on cell culture plates at 37 °C in a humidified incubator at 5% CO_2. To prepare the complete medium, 50 μL of insulin solution was added to the cell culture medium. The complete medium was replaced every two days. MCF-7 (human breast cancer cell line) and PC-3 (human prostate cancer cell line) were cultured in RPMI 1640 medium supplemented with 10% fetal bovine serum (FBS) and 1% antibiotics on cell culture plates at 37 °C in a humidified incubator with 5% CO_2.

2.8 Exosome isolation

For exosome isolation, cell culture supernatants were first collected and centrifuged to remove residual cells and cell debris. Then, 8 mL of the supernatant was transferred to a new microtube and mixed with 4 mL of Exo-spin buffer. The mixture was thoroughly vortexed and incubated at 4 °C for 12 h. Subsequently, 1 mL of the reaction sample solution was centrifuged at 16,000 g for 1 h, and the supernatant was carefully discarded. The pellet containing exosomes was resuspended in 100 μL of PBS. The resuspended exosomes were further purified using an Exo-spin column, according to the manufacturer's instructions, following three steps: (i) incubate the column at room temperature for 15 min to equilibrate the temperature; (ii) remove the lower outlet plug before removing the screw cap, place the Exo-spin column on a waste collection tube, and allow the liquid in the column to drain until near the inner white bead layer; (iii) add 250 μL of PBS to equilibrate the column matrix and allow the buffer to enter the column. Purified exosomes were stored at 4 °C for short-term use or frozen at − 80 °C for long-term storage. To acquire Exo-miRs, 50 μL of 1% Triton X-100 was added, and the mixture was incubated for 10 min at 37 °C for exosome lysis.

2.9 Reverse transcription-quantitative polymerase chain reaction (RT-qPCR)

Before qPCR analysis, cDNA was synthesized from Exo-miRs, and a control miRNA was prepared using a standard poly(A)-tailing-based reverse transcription protocol. Briefly, 2 μL of isolated miRNA was mixed with 2 μL of 10 mM ATP, 2 μL of *E. coli* poly(A) polymerase reaction buffer, 1 μL of *E. coli* poly(A) polymerase (NEB), and 13 μL of DEPC-treated water. The mixture was incubated at 37 °C for 30 min to allow polyadenylation of miRNAs. Next, 10 μL of the tailed miRNAs was mixed with 1 μL of 10 μM universal RT primer and 9 μL of DEPC-treated water, incubated at 70 °C for 5 min, and immediately cooled on ice. For reverse transcription, 10 μL of this mixture was combined with an equal volume (10 μL) of 2× AccuPower RT Master Mix, and the reaction was performed at 42 °C for 60 min, followed by enzyme inactivation at 95 °C for 5 min. The resulting cDNA was subjected to RT–qPCR for target miRNA quantification using a commercial RT–qPCR kit (AccuPower® 2× Greenstar™ qPCR Master Mix, Bioneer, Korea), following the manufacturer's instructions. All amplification reactions were conducted on a Bio-Rad CFX Connect real-time PCR system (USA).

2.10 Clinical sample acquisition

Human plasma samples (*n = 12*) were obtained from Breast cancer patients (B.C.) and healthy donors (H.D.) and supplied by the Biobank of Jeonbuk National University Hospital. The study protocol was reviewed and approved by the Institutional Review Board of Jeonbuk National University Hospital (IRB No.CUH2024-10-039-003). The cohort consisted of six individuals diagnosed with B.C. and six healthy controls. Clinical classification of patient samples was based on pathological evaluation using the TNM staging system in conjunction with human epidermal growth factor receptor 2 (HER2) status. According to the International Classification of Diseases, 10th Revision (ICD-10), B.C. patients were categorized under code C50, whereas healthy participants were assigned code Z00.

3 Results and discussion

3.1 Characterization of synthesized ssRNA–HRP/Au/MoS_2

To construct a nanobiohybrid catalyst platform with high catalytic activity and CRISPR responsiveness, ssRNA–HRP/Au/MoS_2 were synthesized through sequential MoS_2 formation, AuNP deposition, HRP immobilization, and ssRNA functionalization (Fig. 2A). Before Au coating, MoS_2 NPs displayed a characteristic layered morphology with thin, sheet-like domains, as confirmed by TEM analysis (Fig. S1A). These structures provide a high-surface-area scaffold that facilitates catalytic interactions at the nanoscale. Following gold deposition, TEM images revealed a distinct structural transformation in which the MoS_2 surfaces became uniformly decorated with nanoscale Au domains (Figs. 2B and S1B). The emergence of these granular Au features is a key indicator that AuNPs were successfully anchored to the MoS_2 sheets, forming a hybrid Au/MoS_2 structure optimized for enhanced catalytic activity. Elemental analysis using EDS

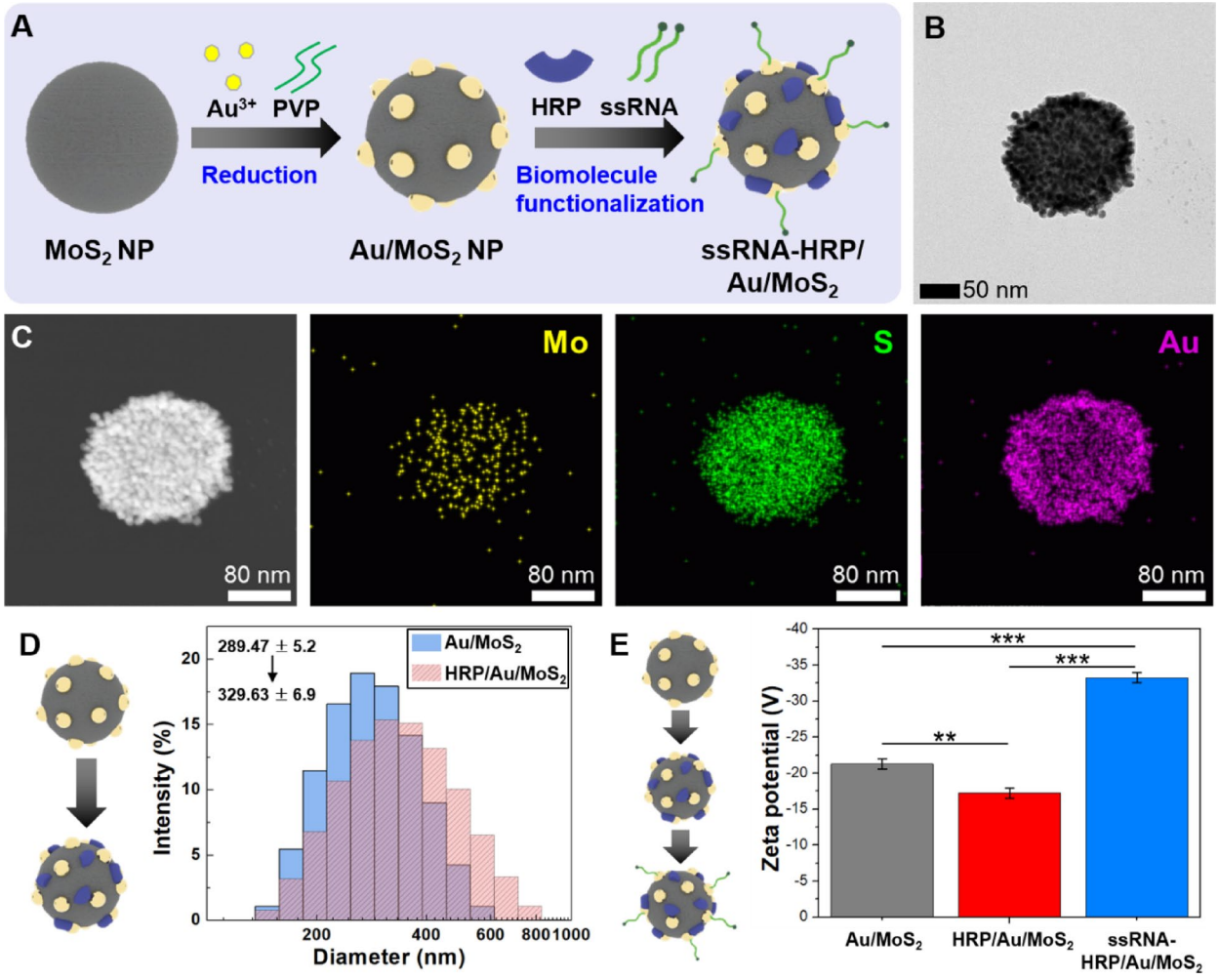


Fig. 2 **A** Schematic illustration of the sequential synthesis and functionalization steps used to construct ssRNA–HRP/Au/MoS_2 nanobiohybrid catalyst. **B** TEM image of Au/MoS_2 NPs. **C** EDS elemental mapping of Mo (yellow), S (green), and Au (pink), confirming uniform Au deposition on the MoS_2 surface. **D** DLS analysis with an increase in hydrodynamic size after HRP conjugation. **E** Zeta potential changes that correspond to sequential modification with HRP and ssRNA, which confirm successful surface functionalization. Statistical significance was determined using one-way ANOVA followed by Tukey's multiple-comparison test (**$P < 0.01$, and ***$P < 0.001$)

spectroscopy further verified the incorporation of Au into the MoS_2 matrix. Whereas pristine MoS_2 exhibited strong Mo and S signals with a consistent atomic ratio of approximately 1:2 (Fig. S1C), the Au/MoS_2 NP displayed an additional distinct Au peak, confirming the introduction of metallic gold.

Importantly, EDS mapping demonstrated that Mo (yellow), S (green), and Au (pink) were uniformly distributed across the nanoparticle surface (Fig. 2C), indicating that Au deposition occurred over the entire MoS_2 structure rather than forming isolated clusters. This uniform coverage is crucial because this strategy supports efficient electron transfer and enhances catalytic turnover during TMB oxidation. To further validate the crystalline nature of the gold coating, X-ray diffraction analysis was conducted at a scan rate of 10°/min over a 2θ range of 10°–80°. Distinct reflections corresponding to the (111), (200), (220), and (311) planes of face-centered cubic Au were observed (Fig. S2), confirming the presence of crystalline gold on the MoS_2 surface. The preservation of MoS_2 stoichiometry together with the appearance of sharp Au peaks collectively demonstrates the formation of a structurally well-defined Au/MoS_2 hybrid nanoparticle with enhanced catalytic potential.

DLS measurements showed an increase in hydrodynamic diameter from 289.47 ± 5.2 nm for Au/MoS_2 to 329.63 ± 6.9 nm after HRP conjugation (Fig. 2D). The PDI values were 0.223 and 0.340 for Au/MoS_2 and HRP/Au/MoS_2, respectively, indicating a moderate broadening of the particle-size distribution following HRP immobilization. The increase in hydrodynamic diameter and the corresponding change in dispersity support the successful formation of the HRP-functionalized nanobiohybrid catalyst. This HRP layer is essential for generating

synergistic catalytic activity when combined with the intrinsic peroxidase-like features of MoS_2 and the electron-transfer properties of gold. In addition, the amount of HRP immobilized on the Au/MoS_2 surface was quantitatively estimated from the difference between the initially added HRP and the unbound HRP remaining in the supernatant after conjugation. Approximately 6.3 μg of HRP was immobilized on 40 μg of Au/MoS_2, corresponding to a loading efficiency of approximately 8.4%. Based on the estimated number of Au/MoS_2 sheets, this loading corresponded to approximately 5.4×10^2 HRP molecules per Au/MoS_2 sheet. Finally, thiol- and biotin-modified ssRNA was introduced onto the HRP/Au/MoS_2 surface to enable CRISPR/Cas13a-triggered release. Zeta-potential measurements confirmed stepwise surface modification: the surface potential increased from − 21.28 ± 0.40 mV for Au/MoS_2 to − 17.22 ± 0.43 mV following HRP immobilization and decreased to − 33.26 ± 0.43 mV after ssRNA attachment (Fig. 2E). These changes reflect predictable alterations in surface charge consistent with protein adsorption and nucleic acid hybridization. The resulting ssRNA–HRP/Au/MoS_2 exhibit a structurally integrated and compositionally uniform architecture ideally suited for strong peroxidase-like activity and CRISPR-responsive activation, providing the basis for a highly efficient colorimetric biosensing system.

3.2 Investigation of amplified colorimetric activity and ssRNA cleavage-dependent behavior of MNB–ssRNA–HRP/Au/MoS_2

The catalytic performance of the synthesized HRP/Au/MoS_2 nanobiohybrid catalyst was first evaluated by comparing the associated TMB oxidation activity with that of MoS_2 and HRP/MoS_2 controls. Visual inspection revealed a clear intensification of blue coloration after the TMB reaction, with HRP/Au/MoS_2 showing the strongest chromogenic output (Fig. 3A). Consistently, ultraviolet–visible (UV–vis) spectroscopy further demonstrated a significantly higher absorbance at 652 nm for HRP/Au/MoS_2 than for MoS_2 or HRP/MoS_2 (Fig. 3B). Quantitative analysis showed a stepwise increase in catalytic activity across the three formulations, confirming that both Au deposition and HRP immobilization contribute synergistically to the overall peroxidase-like function (Fig. 3C). These results establish HRP/Au/MoS_2 as a highly active nanobiohybrid catalyst capable of generating strong and rapid colorimetric signals.

The catalytic mechanism of the HRP/Au/MoS_2 nanobiohybrid was illustrated in Fig. 3D. In the presence of H_2O_2, the HRP/Au/MOS_2 catalyzed the oxidation of TMB into oxidized TMB (oxTMB), producing a strong colorimetric signal. To quantitatively evaluate the catalytic performance, Michaelis–Menten kinetic analyses were performed by varying the concentrations of TMB and H_2O_2 while maintaining the concentration of the other substrate constant (Fig. 3E, F). The kinetic parameters were obtained by nonlinear Michaelis–Menten fitting and were summarized in Table S2. The HRP/Au/MoS_2 nanobiohybrid catalyst exhibited apparent K_m values of 0.880 mM for TMB and 4.81 mM for H_2O_2, indicating substrate affinities comparable to those of free HRP (K_m values of 0.619 mM for TMB and 2.91 mM for H_2O_2). Notably, the corresponding V_{max} values reached 13.5×10^{-8} M s^{-1} for TMB and 20.3×10^{-8} M s^{-1} for H_2O_2, representing substantial increases compared with free HRP (0.915×10^{-8} M s^{-1} for TMB and 0.190×10^{-8} M s^{-1} for H_2O_2). These results suggest that the Au/MoS_2 scaffold does not simply serve as a support for HRP immobilization but significantly enhances catalytic turnover while maintaining efficient substrate recognition. Consequently, the HRP/Au/MoS_2 nanobiohybrid catalyst enables faster oxidation of TMB, leading to rapid color development and amplified colorimetric signal generation.

To evaluate the structural integrity of the magnetic sensing complex, we next examined the morphology of MNB–ssRNA–HRP/Au/MoS_2 complex before ssRNA degradation. In the intact state, TEM and elemental mapping imaging showed that the HRP/Au/MoS_2 were densely clustered around the MNBs, indicating stable conjugation mediated by the streptavidin–biotin–ssRNA linkage (Fig. 3G). However, upon cleavage of the ssRNA linker, the architecture of the complex changed markedly. Meanwhile, treatment with RNase A, used as a model nuclease, caused a clear dispersion of HRP/Au/MoS_2 away from the MNBs (Fig. 3H). The release of individual HRP/Au/MoS_2 into solution confirms that the ssRNA strand functions as an enzymatically cleavable tether that governs HRP/Au/MoS_2 attachment. This cleavage-dependent structural transition was critical for sensor operation because only liberated HRP/Au/MoS_2 can diffuse freely and fully participate in the TMB oxidation reaction, thereby producing a substantially amplified colorimetric signal.

The effect of ssRNA cleavage on catalytic signal generation was further examined by comparing the absorbance of MNB–ssRNA–HRP/Au/MoS_2 complexes under three treatment conditions: control (PBS solution), MNB–ssRNA–HRP/Au/MoS_2 only, and MNB–ssRNA–HRP/Au/MoS_2 treated with RNase A. In both the control and untreated MNB–ssRNA–HRP/Au/MoS_2 groups, negligible absorbance was observed at 652 nm (Fig. 3I). This is because the intact MNB–ssRNA–HRP/Au/MoS_2 complexes were removed from the solution by magnetic separation prior to the TMB reaction, leaving little or no catalyst in the supernatant to drive TMB oxidation, therefore, these groups yield minimal background signals. In contrast, RNase A treatment led to a substantial

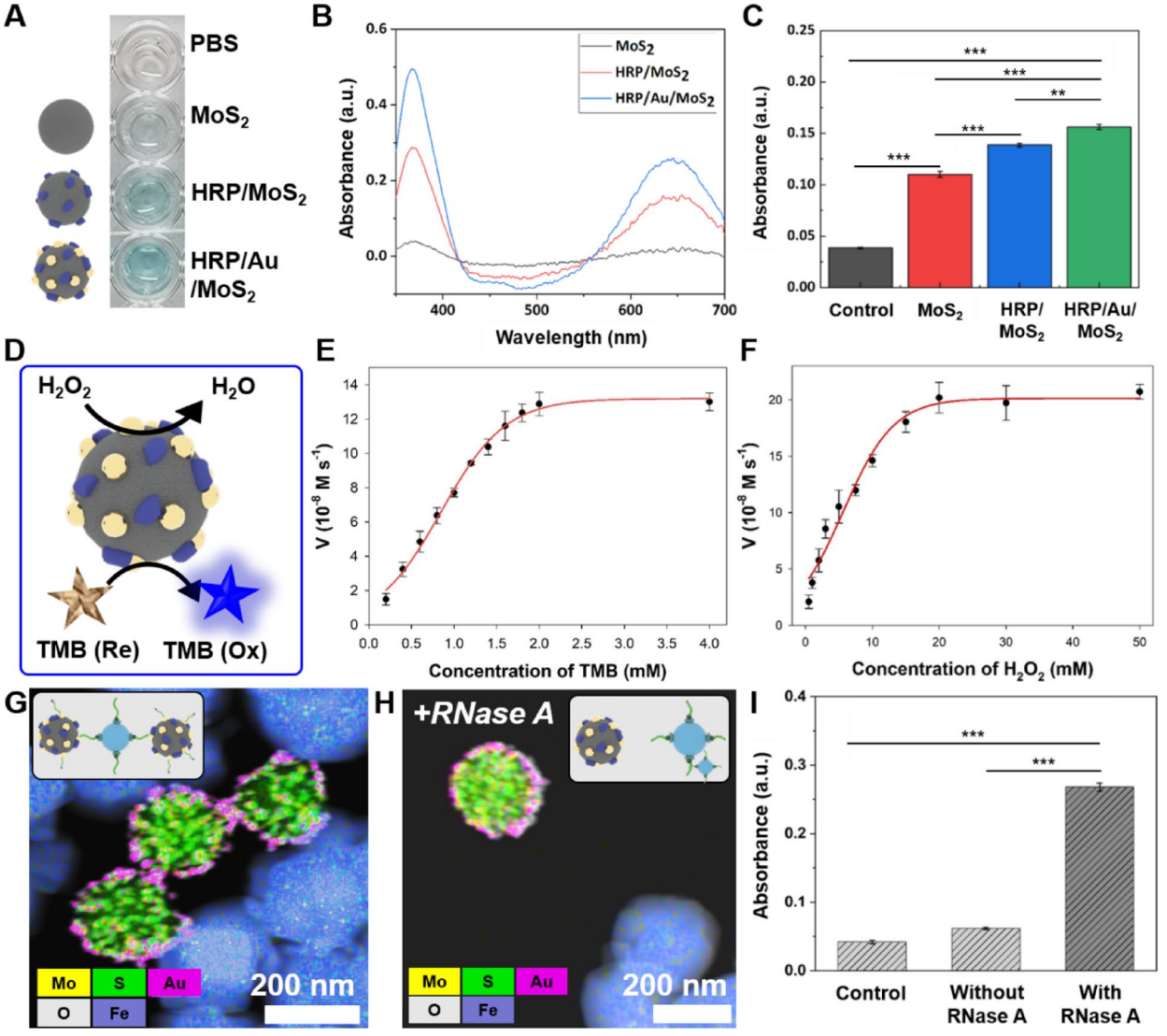


Fig. 3 Investigation of the catalytic properties of HRP/Au/MoS_2 nanobiohybrid catalyst and ssRNA-dependent release behavior of MNB–ssRNA–HRP/Au/MoS_2 complex. **A** Optical images of TMB oxidation catalyzed by MoS_2, HRP/MoS_2, and HRP/Au/MoS_2, which illustrates the enhanced colorimetric response of the nanobiohybrid catalyst. **B** UV–vis absorption spectra of MoS_2, HRP/MoS_2, and HRP/Au/MoS_2. **C** Quantified absorbance at 652 nm demonstrates the synergistic catalytic enhancement of HRP/Au/MoS_2. **D** Schematic illustration of colorimetric signal generation mechanism by the HRP/Au/MoS_2 nanobiohybrid catalyst through the catalytic oxidation of TMB in the presence of H_2O_2. **E** Michaelis–Menten kinetic analysis of the HRP/Au/MoS_2 using varying concentrations of TMB at a fixed H_2O_2 concentration. **F** Michaelis–Menten kinetic analysis of the HRP/Au/MoS_2 nanobiohybrid using varying concentrations of H_2O_2 at a fixed TMB concentration. **G** TEM image and corresponding elemental mapping of the MNB-ssRNA-HRP/Au/MoS_2 complex, showing Mo (yellow), S (green), Au (pink), O (white), and Fe (blue). **H** TEM image and elemental mapping of the MNB-ssRNA-HRP/Au/MoS_2 after RNase treatment, demonstrating the release of HRP/Au/MoS_2 from the MNBs through ssRNA cleavage. **I** Absorbance at 652 nm for control (DEPC), PBS-treated, and RNase A-treated MNB–ssRNA–HRP/Au/MoS_2 complexes, showing that ssRNA cleavage enables HRP/Au/MoS_2 to remain in solution and generate a stronger colorimetric signal. Data are presented as the mean ± standard deviation (SD) from 3 independent experiments. Statistical significance was determined using one-way ANOVA followed by Tukey's multiple-comparison test (**$P < 0.01$, and ***$P < 0.001$)

increase in absorbance intensity. Meanwhile, cleavage of the ssRNA linker by RNase A caused the HRP/Au/MoS_2 to detach from the MNBs and remain in the supernatant during magnetic extraction. These released HRP/Au/MoS_2 readily access the TMB substrate, producing a strong blue coloration and a significant increase in absorbance at 652 nm. This cleavage-dependent increase in signal confirms that HRP/Au/MoS_2 release is the critical activation step governing colorimetric output in this system.

These results confirm that ssRNA cleavage is the key trigger determining whether catalytic HRP/Au/MoS_2 remain in solution and generate a detectable colorimetric signal. This RNase A-based validation establishes the basic release-and-signal principle that will be applied in the CRISPR-based detection system described later.

3.3 Confirmation of CRISPR-enabled activation and analytical performance of the MNB–ssRNA–HRP/Au/MoS_2 sensing platform for miR-155 detection

To confirm that the designed sensing platform specifically responds to target miR-155 via CRISPR/Cas13a activation, the cleavage mechanism was first validated. In this platform, miR-155 hybridizes with the associated complementary crRNA and activates Cas13a, which subsequently induces *trans*-cleavage of the ssRNA (Fig. 4A). This ssRNA cleavage is the essential biochemical trigger that enables HRP/Au/MoS_2 release and initiates downstream colorimetric amplification. The cleavage capability of Cas13a under different reaction conditions was experimentally evaluated by gel electrophoresis (Fig. 4B). Four reaction conditions were tested (excluded (i) ladder in gel): (ii) intact ssRNA without enzyme, (iii) ssRNA incubated with CRISPR/Cas13a in the absence of target miR (inactive condition), (iv) ssRNA incubated with CRISPR/Cas13a activated by miR-155 (active condition), and (v) ssRNA cleaved by RNase A as a degradation control. Intact ssRNA produced a clear band on the gel, which also remained visible when ssRNA was treated with Cas13a in the absence of the target, confirming that CRISPR/Cas13a alone does not induce non-specific ssRNA cleavage. In contrast, ssRNA incubated with Cas13a and target miR-155 showed complete disappearance of the band, indicating that activated CRISPR/Cas13a efficiently cleaved the ssRNA into fragments too small to be retained in the gel. RNase A treatment produced a similar disappearance pattern, validating the complete digestion of ssRNA.

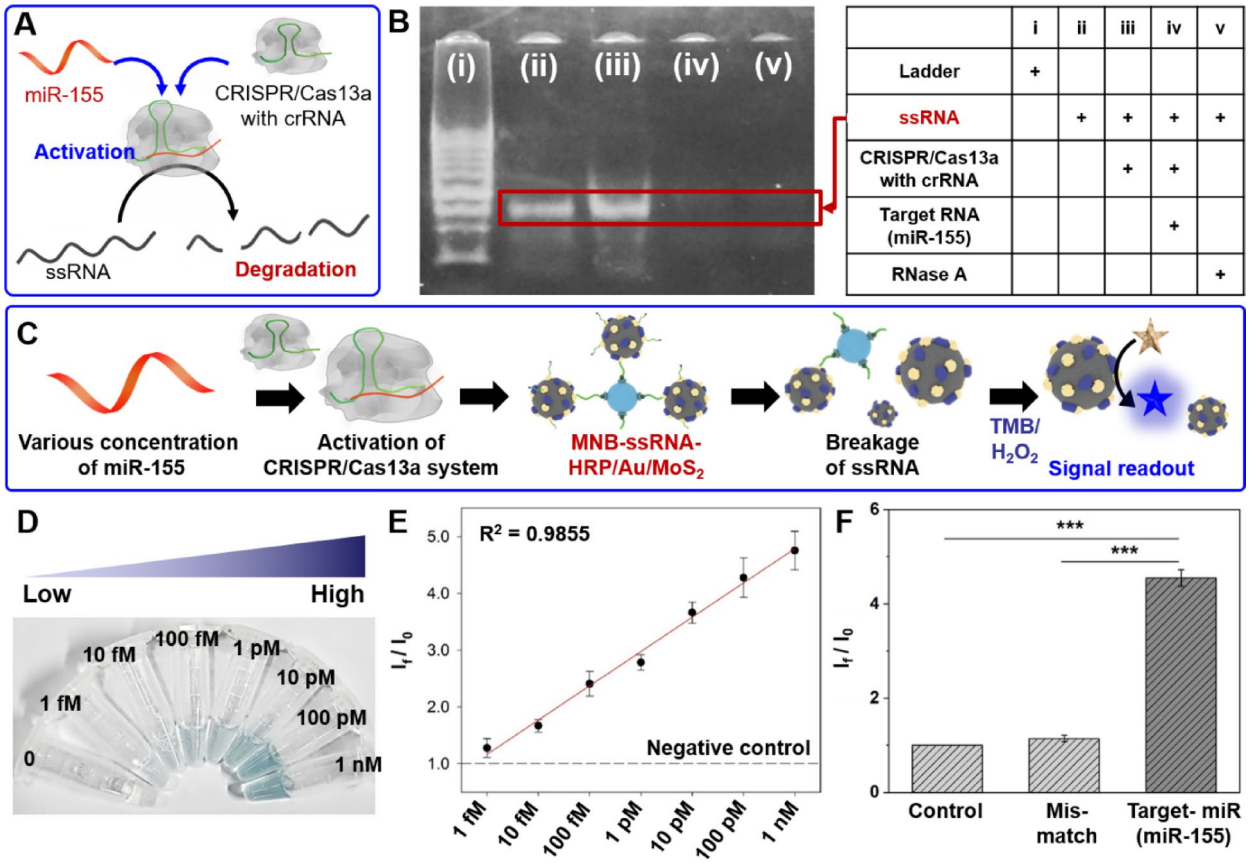


Fig. 4 Confirmation of CRISPR-enabled activation and analytical performance of the MNB–ssRNA–HRP/Au/MoS_2 sensing platform. **A** Schematic illustration of Cas13a activation by the target miR-155 and subsequent collateral cleavage of the ssRNA linker within the MNB–ssRNA–HRP/Au/MoS_2 complex. **B** Gel electrophoresis analysis of ssRNA under four reaction conditions: intact ssRNA (control), ssRNA incubated with inactive Cas13a (without target), ssRNA cleaved by activated Cas13a (with target miR-155), and ssRNA completely cleaved by RNase A. **C** Schematic illustration of concentration-dependent Cas13a activation leading to ssRNA cleavage and HRP/Au/MoS_2 release for colorimetric detection. **D** Visual colorimetric responses of the sensing system at various miR-155 concentrations (control, 1 fM, 10 fM, 100 fM, 1 pM, 10 pM, 100 pM, 1 nM) after 30 min of reaction. **E** Quantitative absorbance analysis, with a strong linear correlation between normalized signal (I_f/I_0) and miR-155 concentration (1 fM–1 nM), with a limit of detection (LOD) of 0.82 fM, calculated using the 3σ/s method based on 10 independent blank measurements ($n = 10$). **F** Specificity assessment, which demonstrates that only the perfectly matched target miR-155 activates Cas13a and induces ssRNA cleavage, whereas a single-base-mismatched miR does not produce a detectable signal. Data are presented as the mean ± standard deviation (SD) from 3 independent experiments. Statistical significance was determined using one-way ANOVA followed by Tukey's multiple-comparison test (***$P < 0.001$)

Based on these results, we incorporated our MNB–ssRNA–HRP/Au/MoS_2 complex into a CRISPR/Cas13a-based biosensing system for miR-155 detection (Fig. 4C). Upon the addition of target miR-155 and the associated complementary crRNA, CRISPR/Cas13a becomes activated and induces collateral cleavage of the ssRNA linker within the MNB–ssRNA–HRP/Au/MoS_2 complex. Cleavage of this linker releases the HRP/Au/MoS_2 from the MNBs, allowing these particles to remain in solution after magnetic extraction and catalyze TMB oxidation. This cleavage-triggered retention of nanozymes in solution is the fundamental principle enabling quantitative, amplification-free colorimetric detection of the target miRNA. Importantly, before the analytical evaluation, key experimental parameters that affect signal generation were systematically optimized to ensure reliable and sensitive detection. The TMB reaction time was first optimized to balance signal development and background increase. Although the colorimetric signal increased with reaction time, incubations longer than 30 min led to a significant increase in the background signal (I_0), reducing the signal-to-background ratio (I_f/I_0) (Fig. S3). Therefore, 30 min was selected as the optimal TMB reaction time for subsequent experiments. In addition, the *trans*-cleavage activity of CRISPR/Cas13a was optimized at different temperatures (Fig. S4). The colorimetric responses varied with temperature, reflecting the temperature-dependent kinetics of Cas13a activation and collateral cleavage. The condition that produced the highest signal output (37 °C) was selected for further experiments. Moreover, the effect of reaction time on Cas13a trans-cleavage activity was evaluated (Fig. S5). The signal intensity increased with incubation time due to progressive ssRNA cleavage and HRP/Au/MoS_2 release, but reached a maximum level beyond a certain time point. Therefore, an optimal reaction time of 60 min was selected to achieve efficient cleavage while maintaining overall assay time efficiency. Based on these optimized conditions, subsequent experiments were performed to evaluate the analytical performance of the proposed sensing platform.

To visually assess the ability of the platform to distinguish varying miR-155 concentrations, colorimetric analysis was performed across a series of target levels (control, 1 fM, 10 fM, 100 fM, 1 pM, 10 pM, 100 pM, 1 nM) (Fig. 4D). After a 30 min reaction period, progressively more intense blue coloration was observed with increasing miR-155 concentration, demonstrating that even femtomolar-level inputs were sufficient to activate Cas13a and release measurable amounts of catalytic HRP/Au/MoS_2. This visually distinguishable signal arises from the high catalytic activity of the HRP/Au/MoS_2, which produces strong TMB oxidation without requiring additional nucleic acid amplification. The naked-eye detectability demonstrates the potential of the platform for qualitative visual detection. For quantitative analysis, absorbance responses were measured across a broader range of miR-155 concentrations (1 fM–1 nM) (Fig. 4E). The normalized absorbance (I_f/I_0) increased proportionally with target concentration, exhibiting a strong linear correlation (R^2 = 0.9855) (y = 0.6036 x + 1.165, x = log [miR-155 concentration (fM)]). This concentration-dependent signal enhancement confirms that the extent of HRP/Au/MoS_2 release is directly governed by the level of Cas13a activation, thereby enabling accurate quantification of the target miRNA. The LOD was calculated using the 3σ/s method, where σ represents the standard deviation of 10 independent blank measurements (n = *10*) and s represents the slope of the calibration curve. The resulting LOD was 0.82 fM. This result demonstrated high analytical sensitivity comparable to or exceeding that of existing CRISPR-based colorimetric assays. This low LOD reflects the synergistic catalytic amplification provided by the HRP/Au/MoS_2 and the efficient cleavage-triggered release mechanism inherent to the MNB–ssRNA–HRP/Au/MoS_2 platform.

To evaluate the reproducibility of the complete analytical procedure, intra-assay and inter-assay precision were examined at two representative miR-155 concentrations (100 fM and 10 pM). The intra-assay CVs were 13.51% and 17.31% at 100 fM and 10 pM, respectively, while the corresponding inter-assay CVs were 21.74% and 24.50%. These results indicate acceptable within-assay precision, although greater variability was observed between independently prepared assay batches. The detailed results are summarized in Table S3. Based on these analytical validation results, the overall performance of the proposed platform was further compared with previously reported CRISPR-based colorimetric miRNA detection methods. Compared with previously reported CRISPR/Cas13a-based colorimetric biosensors, the proposed biosensor provides a broad target RNA detection range and a low LOD without requiring nucleic acid amplification, owing to the enhanced signal generated by the synergistic catalytic activity of HRP/Au/MoS_2 (Table 1).

The specificity of CRISPR-mediated cleavage was next examined using a single-base-mismatched miR sequence (Fig. 4F). While the target miR-155 successfully activated Cas13a and generated a strong absorbance signal via ssRNA cleavage, the one-mismatched miR failed to induce detectable cleavage or signal enhancement, yielding responses comparable to the inactive control. These results confirm that Cas13a activation in this system is strictly target-dependent and can discriminate against single-nucleotide variations, a crucial requirement for reliable miR detection. This high specificity arises from the RNA-guided recognition mechanism of Cas13a and ensures that nonspecific binding or off-target cleavage does not compromise analytical performance.

Table 1 Comparative analysis of previously reported amplification-free, CRISPR-based colorimetric methods for miRNA detection

Biosensor	Method	Target	Time (min)	Detection range	LOD	Refs.
Hemin entropy-driven amplification (EDA) with CRISPR–Cas13a	Colorimetric	miR-21	95	50 pM–1 nM	5.12 pM	[24]
Hemin aptamer's peroxidase activity with CRISPR–Cas12a	Colorimetric	miR-210-3p	100	1 pM–50 nM	0.95 pM	[25]
MB–ssDNA–Pt@Au probes with CRISPR–Cas12a	Colorimetric	miR-21	95	1 pM–500 pM	0.5 pM	[26]
CRISPR/Cas13a and MnO_2 nanosheets-mediated recognition and signal amplification	Colorimetric	miR-21	10	1–50 pM	0.33 pM	[27]
MB30–RNA1–MM1000 with CRISPR/Cas13a system	Colorimetric	miR-21	60	1 pM–50 nM	0.22 pM	[28]
$NiCo_2O_4$ nanoenzyme by Mn doping with CRISPR/Cas13a	Colorimetric	miR-21	90	500 fM–10 nM	0.21 pM	[29]
CRISPR/Cas12a system and exonuclease-assisted target recycling signal amplification	Colorimetric	miR-141	165	200 fM–10 nM	62 fM	[30]
MB–ssDNA–GOx with CRISPR–Cas12a	Colorimetric	miR-205	130	50 fM–50 pM	36.4 fM	[31]
HRP-mimicking G-quadruplex/hemin complexes with CRISPR–Cas13a	Colorimetric	miR-21	85	50 fM–1 nM	27 fM	[32]
CRISPR–Cas13a system with an exonuclease-iii (Exo-iii)-assisted chain cleavage of silver ions (Ag^+)-aptamer and an Ag^+-based color reaction	Colorimetric	miR-155	75	5 fM–100 pM	5.12 fM	[33]
CRISPR/Cas12a with alkaline phosphatase (ALP)-mediated signal enhancement	Colorimetric	miR-106b-5p	190	100 fM–10 pM	7.16 fM	[34]
		miR-9			3.34 fM	
MNB–ssRNA–HRP/Au/MoS_2 complex with CRISPR/Cas13a	**Colorimetric**	**miR-155**	**90**	**1 fM–1 nM**	**0.82 fM**	**This study**

The storage stability of the assembled MNB–ssRNA–HRP/Au/MoS_2 complex was further evaluated at 4 °C for up to 13 days (Fig. S6). During storage, only background-level signals were observed in the supernatant after magnetic separation, indicating negligible spontaneous release of HRP/Au/MoS_2 from the magnetic complex. Importantly, the complex retained a strong target-responsive signal after 13 days when challenged with 100 pM miR-155 in the CRISPR/Cas13a assay. These results demonstrate that the assembled sensing complex maintains its structural and functional stability for at least 13 days under refrigerated storage conditions.

To further investigate the versatility of the sensing architecture, a proof-of-concept DNA detection assay was additionally constructed using CRISPR/Cas12a (Fig. S7). In this system, the ssRNA linker used in the Cas13a-based system was replaced with an ssDNA linker, and a BRCA1-derived DNA sequence was employed as the model target together with the corresponding Cas12a crRNA (Table S4). At a target concentration of 100 nM, the target DNA induced a markedly increased colorimetric signal, whereas the PBS control and non-target miR-155 produced only background-level responses. These results demonstrate that the proposed sensing architecture is not restricted to Cas13a-mediated RNA detection and can be adapted to DNA targets by changing the CRISPR effector, guide RNA, and cleavable linker while retaining the HRP/Au/MoS_2-based colorimetric signal-generation strategy.

3.4 Exo-miR-155 detection in cell-derived samples using the MNB–ssRNA–HRP/Au/MoS_2 complex with CRISPR/Cas13a system

To evaluate the applicability of the proposed colorimetric biosensor in a biologically relevant context, Exo-miR-155 was extracted from three representative cell lines and analyzed using the MNB–ssRNA–HRP/Au/MoS_2 complex-based sensing platform: MCF-10A (non-tumorigenic epithelial cell line), PC-3 (prostate cancer cell line), and MCF-7 (BC cell line). This workflow demonstrates the complete detection process, from exosome isolation to CRISPR-mediated activation and signal generation (Fig. 5A).

Representative optical microscopy images of the three cell lines confirm healthy and distinct cellular morphologies (Fig. 5B–D). Exosomes isolated from each cell line were subsequently characterized by Fluorescence Nanoparticle Tracking Analysis (FL-NTA) to verify their size distribution (Fig. 5E–G). All samples exhibited a dominant peak within the 50–250 nm range, consistent with the expected dimensions of exosomal vesicles, thereby confirming successful extraction of intact exosomes from each suitable cell line for downstream Exo-miR analysis [35, 36]. TEM imaging further validated the morphology of the isolated vesicles, revealing well-defined spherical structures with characteristic lipid bilayer membranes (Fig. 5H). The preservation of vesicle integrity throughout the isolation process was essential for ensuring accurate quantification of endogenous Exo-miRs.

To determine whether the sensing platform could distinguish Exo-miR-155 levels in exosomes derived from different cell lines, colorimetric responses were measured after CRISPR/Cas13a activation by Exo-miR extracts.

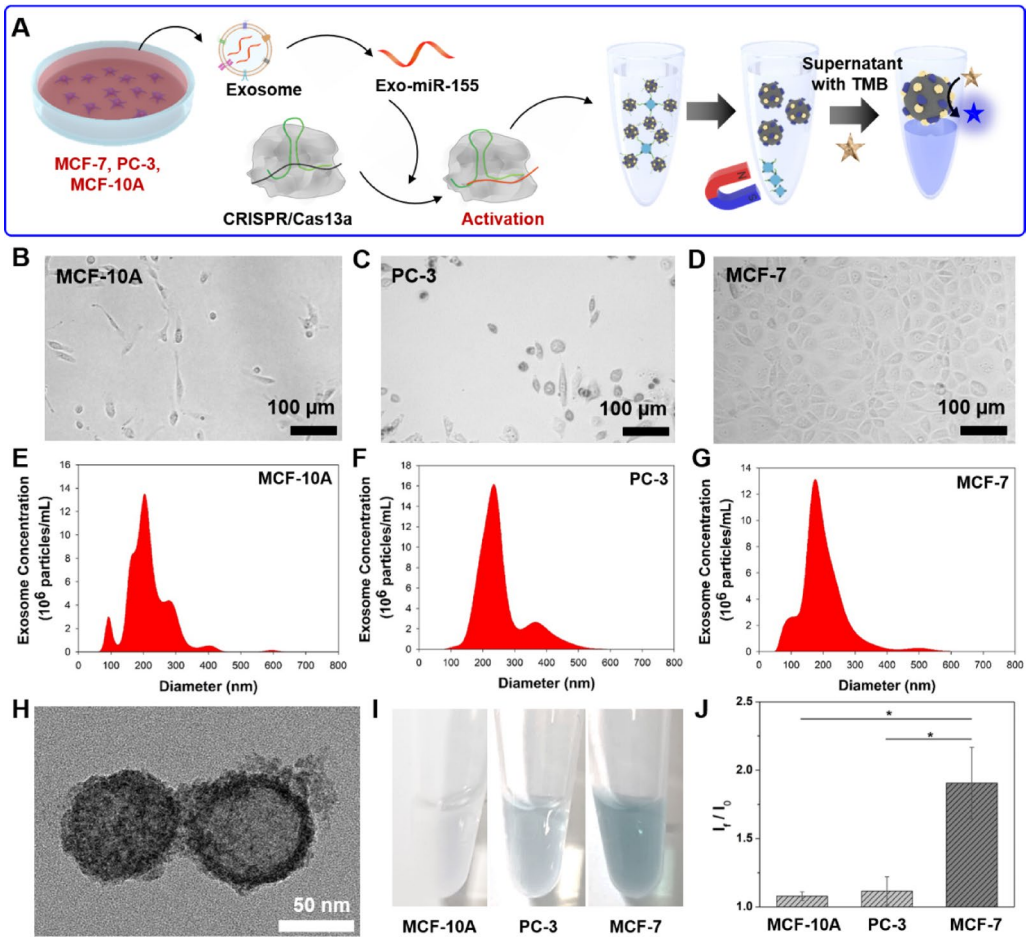


Fig. 5 Detection of Exo-miR-155 from cell-derived samples using the CRISPR/Cas13a-enabled MNB–ssRNA–HRP/Au/MoS_2 sensing platform. **A** Schematic illustration of the workflow for exosome isolation from MCF-10A, PC-3, and MCF-7 cells and subsequent detection of Exo-miR-155 via Cas13a-mediated ssRNA cleavage and colorimetric signal generation. Optical microscopy images of **B** MCF-10A, **C** PC-3, and **D** MCF-7 cells used for exosome collection. FL-NTA size-distribution profiles of exosomes isolated from **E** MCF-10A, **F** PC-3, and **G** MCF-7 cells, with characteristic vesicle sizes (50–250 nm) (*n* = *3*). **H** TEM image of isolated exosomes confirming intact spherical vesicle morphology. **I** Visual colorimetric responses of the sensing platform for Exo-miR-155 analysis in exosomes from the three cell lines. **J** Quantified normalized signals (I_f/I_0) revealing higher Exo-miR-155 levels in MCF-7-derived exosomes compared with those from PC-3 and MCF-10A, consistent with elevated miR-155 expression in breast cancer cells. Data are presented as the mean ± standard deviation (SD) from 3 independent experiments. Statistical significance was determined using one-way ANOVA followed by Tukey's multiple-comparison test (*$P < 0.05$)

The blue coloration intensified markedly with exosome source (Fig. 5I), with MCF-7 exosomes eliciting the strongest visual response. Quantitative measurements confirmed this trend, yielding normalized signal values of 1.905 for MCF-7, 1.117 for PC-3, and 1.079 for MCF-10A (Fig. 5J). These differences align with known expression profiles: Exo-miR-155 is highly upregulated in BC cells, whereas Exo-miR-155 abundance is much lower in prostate cancer and non-tumorigenic epithelial cells. Therefore, the elevated signal from MCF-7 exosomes reflects enhanced Cas13a activation driven by the higher associated Exo-miR-155 content, resulting in more extensive ssRNA cleavage and increased release of HRP/Au/MoS_2 into solution. In contrast, the minimal responses observed in PC-3 and MCF-10A exosomes highlight the selectivity of the platform for physiologically relevant variations in miR-155 expression.

Importantly, these distinctions were detected without any nucleic acid amplification, underscoring the inherent sensitivity of the HRP/Au/MoS_2-amplified colorimetric readout. Collectively, these results demonstrate that the MNB–ssRNA–HRP/Au/MoS_2 system, coupled with CRISPR/Cas13a, can reliably quantify Exo-miR-155 directly from cell-derived exosomes. Moreover, before applying the sensing platform to clinical samples, the potential contribution of matrix-derived peroxidase-like activity to the TMB/H_2O_2 readout was evaluated using plasma and cell culture medium (Fig. S8). Direct reaction of plasma with TMB/H_2O_2 produced a substantial background signal, indicating the presence of endogenous components with peroxidase-like activity. However, this

signal was markedly reduced after exosome isolation, and negligible responses were observed from both isolated exosomes and lysed exosome fractions. In contrast, when the lysed exosome samples were analyzed using the complete CRISPR/Cas13a-based sensing platform, a significant colorimetric signal was generated. In cell culture medium, negligible intrinsic TMB oxidation was observed before and after exosome isolation and lysis, whereas a strong colorimetric response was obtained after analysis with the complete sensing platform. These results indicate that matrix-derived peroxidase-like activity is effectively minimized during exosome isolation and does not substantially contribute to the final analytical signal, which predominantly originates from CRISPR/Cas13a-triggered release of the HRP/Au/MoS_2 catalyst. This application-level validation confirms the strong potential of the platform for Exo-miR profiling and supports the associated broader utility in cancer diagnostics and other biomedical analyses.

3.5 Performance of the MNB–ssRNA–HRP/Au/MoS_2 complex with the CRISPR/Cas13a system in clinical samples

To evaluate the clinical applicability of the MNB–ssRNA–HRP/Au/MoS_2 platform combined with the CRISPR/Cas13a system, we applied the assay to detect Exo-miR-155 in human plasma samples from B.C. patients ($n = 6$) and H.D. ($n = 6$) obtained from the Biobank of Jeonbuk National University Hospital (Fig. 6A). The B.C. cohort included patients with TNM stages ranging from T1bN0 to T2N2a, and all six patients were HER2-negative, as summarized in Table S5. This study was approved by the Institutional Review Board of Jeonbuk National University Hospital (IRB number: CUH2024-10-039-003) and was conducted in accordance with the Declaration of Helsinki. The Biobank of Jeonbuk National University Hospital obtained written informed consent from all participants.

The colorimetric responses (I_f/I_0) obtained from the clinical samples are presented in Fig. 6B. Notably, plasma samples from B.C. patients consistently exhibited higher signal intensities than those from H.D., reflecting elevated Exo-miR-155 levels associated with tumor progression. The difference between the two groups was clearly distinguishable across all samples, with no observable overlap in signal, indicating strong intrinsic diagnostic separability of the platform. Although the colorimetric response can be visually observed, quantitative discrimination between the B.C. and H.D. groups in this study was based on absorbance measurements using a microplate reader. To quantitatively assess statistical significance, scatter dot plot analysis was performed (Fig. 6C). The results revealed a highly significant difference between the B.C. and H.D. groups (***$P < 0.001$, Student's t-test), confirming that the MNB–ssRNA–HRP/Au/MoS_2 platform with the CRISPR/Cas13a-based colorimetric system can reliably differentiate disease states in clinical samples.

To further validate analytical accuracy, expression profiles obtained from the colorimetric assay were compared with those measured by RT-qPCR. As shown in the heatmap, the Exo-miR-155 expression patterns across individual samples were highly consistent between the two methods (Fig. 6D). To quantitatively assess the agreement between the two methods, Pearson correlation analysis was performed using the 12 individual clinical samples. A strong positive correlation was observed between the colorimetric signals and RT-qPCR measurements (Pearson's $r = 0.961$, $p < 0.001$, $n = 12$) (Fig. S9). These results demonstrate that the proposed platform provides Exo-miR-155 measurements that are highly consistent with those obtained using conventional RT-qPCR. Finally, receiver operating characteristic (ROC) curve analysis was performed to evaluate the diagnostic performance of the platform (Fig. 6E). The system achieved an area under the curve (AUC) of 1.00 in the tested cohort, demonstrating promising diagnostic discrimination between the B.C. and H.D. groups. However, given the limited cohort size ($n = 6$ per group), this result should be considered a pilot-scale clinical validation, and further studies involving larger and more diverse patient cohorts are required to establish the diagnostic performance of the proposed platform.

Despite the promising analytical and preliminary clinical performance, the current platform remains a laboratory-scale assay involving several manual steps, including exosome isolation, incubation, and magnetic separation. Furthermore, although the colorimetric response enables qualitative visual observation, quantitative analysis in the present study requires absorbance measurement using a microplate reader. Further integration and simplification of sample preparation, reaction, separation, and quantitative readout will therefore be required for future translation of the proposed platform into a practical point-of-care format.

Overall, these results demonstrate the feasibility of applying the MNB–ssRNA–HRP/Au/MoS_2 platform combined with CRISPR/Cas13a to Exo-miR-155 detection in clinical samples. The observed differences between the B.C. and H.D. groups in this pilot cohort support further investigation of the platform in larger clinical studies.

4 Conclusion

This study developed an amplification-free colorimetric biosensing platform for Exo-miR-155 detection by integrating CRISPR/Cas13a with a highly active HRP/Au/MoS_2 nanobiohybrid catalyst. The engineered HRP/Au/MoS_2 exhibits markedly enhanced chromogenic performance by combining the catalytic turnover of HRP,

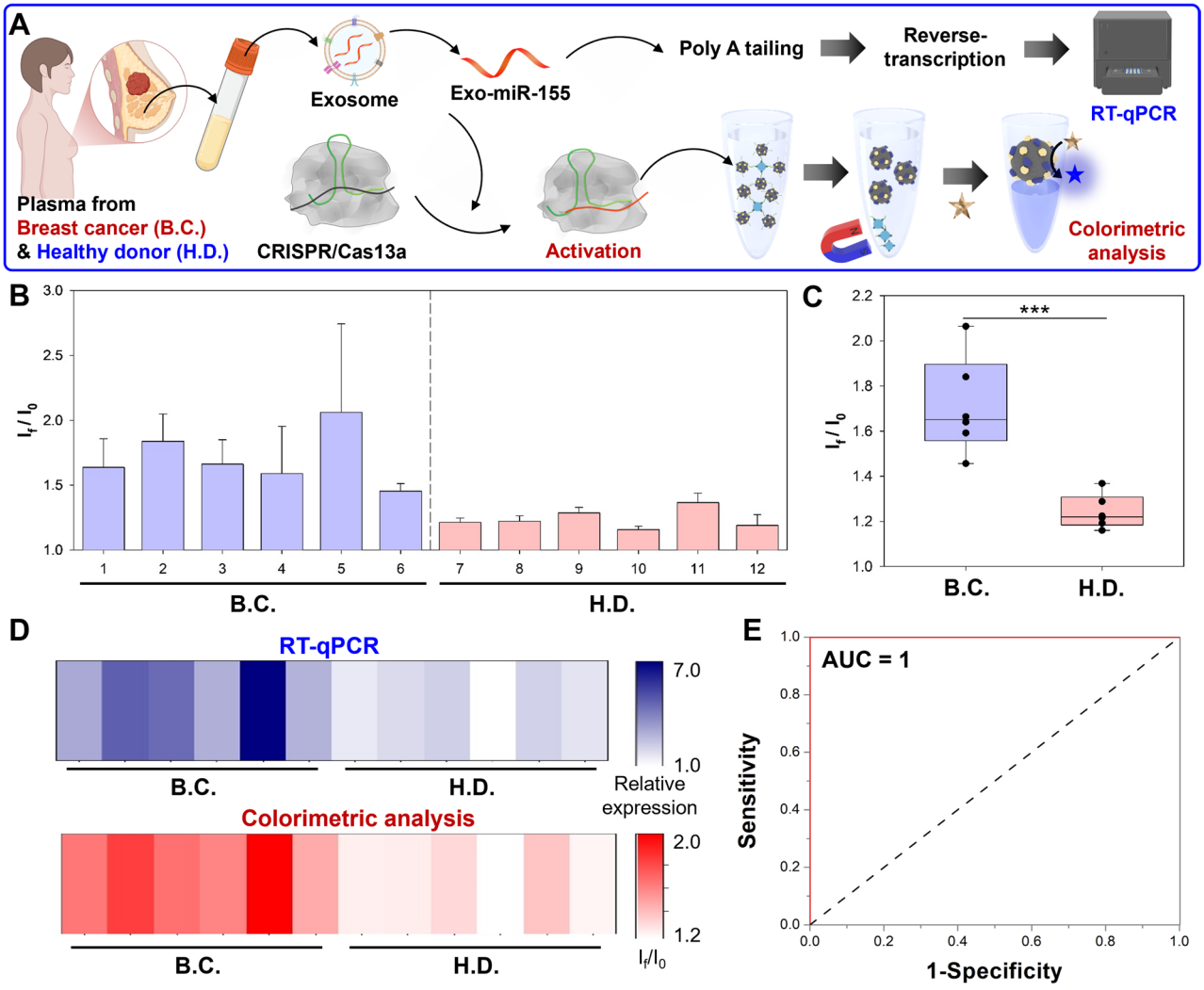


Fig. 6 Detection of Exo-miR-155 in clinical samples (breast cancer: $n = 6$; healthy donors: $n = 6$) using the MNB–ssRNA–HRP/Au/MoS_2 CRISPR/Cas13a system. **A** Schematic illustration of the workflow for Exo-miR-155 detection from clinical plasma samples, comparing the colorimetric method (CRISPR/Cas13a-enabled MNB–ssRNA–HRP/Au/MoS_2 sensing platform) with the conventional RT-qPCR approach. **B** Colorimetric responses from plasma-derived Exo-miR-155 obtained using the MNB–ssRNA–HRP/Au/MoS_2 CRISPR/Cas13a system. **C** Scatter dot plots of the statistical analysis of colorimetric signals measured using the MNB–ssRNA–HRP/Au/MoS_2 CRISPR/Cas13a system. **D** Heatmap representation of Exo-miR-155 levels in plasma samples. Relative expression levels determined by RT-qPCR (blue) are compared with colorimetric signals (I_f/I_0) obtained by the MNB–ssRNA–HRP/Au/MoS_2 CRISPR/Cas13a system (red). **E** Receiver operating characteristic (ROC) curve analysis evaluating the diagnostic performance of Exo-miR-155 detection with the MNB–ssRNA–HRP/Au/MoS_2 CRISPR/Cas13a system. Data are presented as the mean ± standard deviation (SD) from 3 independent experiments. Statistical significance was determined using Student's t-test (***$P < 0.001$)

the electron-transfer efficiency of AuNPs, and the high-surface-area scaffold with peroxidase-like activity of MoS_2. By coupling this HRP/Au/MoS_2 with an ssRNA-tethered MNB architecture, CRISPR/Cas13a-mediated collateral cleavage was effectively translated into HRP/Au/MoS_2 release and robust colorimetric signal generation. The proposed system achieved high attomole-level sensitivity, a wide dynamic range, and single-nucleotide specificity without requiring nucleic acid amplification or complex instrumentation. Importantly, the platform successfully distinguished Exo-miR-155 levels in exosomes derived from different cell lines, demonstrating the applicability of this system to biologically relevant samples and an ability to reflect established cancer-associated expression patterns. These findings highlight that enhancing the intrinsic signal strength of colorimetric systems through rational HRP/Au/MoS_2 engineering can effectively overcome the sensitivity limitations that have traditionally restricted amplification-free assays. Overall, this CRISPR-enabled, HRP/Au/MoS_2-based colorimetric strategy offers a simple, sensitive, and instrument-free approach for Exo-miR analysis. Owing to the modular design of the platform, this system can be readily adapted to other RNA targets by reprogramming the

crRNA sequence, highlighting the strong potential of the platform for point-of-care early cancer diagnostics and broader nucleic acid sensing applications.

Supplementary Information

The online version contains supplementary material available at https://doi.org/10.1186/s40580-026-00580-y.

Supplementary Material 1

Acknowledgements
Not applicable.

Author contributions
M.-J. Lee and M. Shin contributed equally to this work. M.-J. Lee: investigation, formal analysis, visualization, writing—original draft and editing; M. Shin: investigation, formal analysis, visualization, writing—original draft and editing; J. Lim: investigation; H.R. Ahn: investigation, resources; D. Jung: investigation; S. Liu: investigation; C. Li: investigation; J.-H. Choi: conceptualization, supervision, methodology, writing—review and editing; J.-W. Choi: conceptualization, supervision, writing—review and editing. J.-W. Choi and J.-H. Choi are co-corresponding authors.

Funding
This work was supported by the National Research Foundation of Korea (NRF) grant funded by the Korea government (MSIT) (RS-2024-00344633), by the Basic Research Laboratory through the National Research Foundation of Korea grant funded by the Ministry of Science and ICT (Grant number RS-2026-25509643), and by Jeonbuk National University, granted financial resources from HYUNSONG Educational & Cultural Foundation. The biospecimens and data used in this study were provided by the Biobank of Jeonbuk National University Hospital, a member of the Korea Biobank Network, which is supported by the Ministry of Health, Welfare, and Family Affairs. All samples derived from the Korea Biobank Network were obtained with informed consent and in accordance with institutional review board-approved protocols.

Data availability
The data that support the findings of this study are available from the corresponding author upon reasonable request.

Declarations

Ethics approval and consent to participate
This study was approved by the Institutional Review Board of Jeonbuk National University Hospital (IRB number: CUH2024-10-039-003) and was conducted in accordance with the Declaration of Helsinki.

Competing interests
The authors declare that they have no known competing financial interests or personal relationships that could have appeared to influence the work reported in this paper.

Author details
[1]Department of Chemical & Biomolecular Engineering, Sogang University, 35, Baekbeom-ro, Mapo-gu, Seoul 04107, Republic of Korea
[2]Department of Chemical Engineering, Research Center of Chemical Technology, Hankyong National University, Gyeonggi–do 17579, Republic of Korea
[3]Department of Surgery, Jeonbuk National University Medical School, Jeonju-si 54907, Republic of Korea
[4]Sichuan Provincial Key Laboratory for Human Disease Gene Study, Department of Medical Genetics, Sichuan Academy of Medical Sciences & Sichuan Provincial, People's Hospital, University of Electronic Science and Technology of China, Chengdu 610072, China
[5]Biomedical Engineering, School of Medicine, The Chinese University of Hong Kong, Shenzhen 518172, China
[6]School of Chemical Engineering, Jeonbuk National University, 567, Baekje-daero, Deokjin-gu, Jeonju-si, Jeollabuk-do 54896, Republic of Korea

Received: 29 July 2026 / Accepted: 22 September 2026
Published online: 30 September 2026

References

1. M. Alexander, R. Hu, M.C. Runtsch, D.A. Kagele, T.L. Mosbruger, T. Tolmachova, M.C. Seabra, J.L. Round, D.M. Ward, R.M. O'Connell, Exosome-delivered microRNAs modulate the inflammatory response to endotoxin. Nat. Commun. **6**, 7321 (2015). https://doi.org/10.1038/ncomms8321
2. H. Valadi, K. Ekström, A. Bossios, M. Sjöstrand, J.J. Lee, J.O. Lötvall, Exosome-mediated transfer of mRNAs and microRNAs is a novel mechanism of genetic exchange between cells. Nat. Cell Biol. **9**, 654–659 (2007). https://doi.org/10.1038/ncb1596
3. A. Thind, C. Wilson, Exosomal miRNAs as cancer biomarkers and therapeutic targets. J. Extracell. Vesicles **5**, 31292 (2016). https://doi.org/10.3402/jev.v5.31292
4. M. Salehi, M. Sharifi, Exosomal miRNAs as novel cancer biomarkers: challenges and opportunities. J. Cell. Physiol. **233**, 6370–6380 (2018). https://doi.org/10.1002/jcp.26481
5. S. Chen, T. Jiang, H. Lin, J. Chen, S. Yang, P. Wang, X. Gan, Y. Wang, B. Xu, J. Sun, C. Yin, Z. Huang, Y. Fang, Fast and ultrasensitive visual detection of exosomes in body fluids for point-of-care disease diagnosis. Anal. Chem. **93**, 10372–10377 (2021). https://doi.org/10.1021/acs.analchem.1c02136
6. W. Ando, K. Kikuchi, T. Uematsu, H. Yokomori, T. Takaki, M. Sogabe, Y. Kohgo, K. Otori, S. Ishikawa, I. Okazaki, Novel breast cancer screening: combined expression of miR-21 and MMP-1 in urinary exosomes detects 95% of breast cancer without metastasis. Sci. Rep. **9**, 13595 (2019). https://doi.org/10.1038/s41598-019-50084-5
7. Z. Zhang, L. Zhang, G. Yu, Z. Sun, T. Wang, X. Tian, X. Duan, C. Zhang, Exosomal miR-1246 and miR-155 as predictive and prognostic biomarkers for trastuzumab-based therapy resistance in HER2-positive breast cancer. Cancer Chemother. Pharmacol. **86**, 761–772 (2020). https://doi.org/10.1007/s00280-020-04168-z
8. D.D. Liu, B.B. Li, X.S. Shi, J.X. Zhang, A.M. Chen, J.R. Xu, W. Wang, K.L. Huang, J.W. Gao, Z.X. Zheng, D. Liu, H.M. Wang, W. Shi, L. Chen, J.H. Xu, Cross-platform genomic identification and clinical validation of breast cancer diagnostic biomarkers. Aging **13**, 4258–4273 (2021). https://doi.org/10.18632/aging.202388
9. X. Huang, T. Yuan, M. Tschannen, Z. Sun, H. Jacob, M. Du, M. Liang, R.L. Dittmar, Y. Liu, M. Liang, M. Kohli, S.N. Thibodeau, L. Boardman, L. Wang, Characterization of human plasma-derived exosomal RNAs by deep sequencing. BMC Genomics **14**, 319 (2013). https://doi.org/10.1186/1471-2164-14-319
10. J.R. Chevillet, Q. Kang, I.K. Ruf, H.A. Briggs, L.N. Vojtech, S.M. Hughes, H.H. Cheng, J.D. Arroyo, E.K. Meredith, E.N. Gallichotte, E.L. Pogosova-Agadjanyan, C. Morrissey, D.L. Stirewalt, F. Hladik, E.Y. Yu, C.S. Higano, M. Tewari, Quantitative and stoichiometric analysis of the microRNA content of exosomes. Proc. Natl. Acad. Sci. U. S. A. **111**, 14888–14893 (2014). https://doi.org/10.1073/pnas.1408301111
11. Y. Wu, Y. Zhang, X. Zhang, S. Luo, X. Yan, Y. Qiu, L. Zheng, L. Li, Research advances for exosomal miRNAs detection in biosensing: from the massive study to the individual study. Biosens. Bioelectron. **177**, 112962 (2021). https://doi.org/10.1016/j.bios.2020.112962
12. Q. Feng, W. Fan, W. Ren, C. Liu, Recent advances in exosome analysis assisted by functional nucleic acid-based signal amplification technologies. TrAC Trends Anal. Chem. **149**, 116549 (2022). https://doi.org/10.1016/j.trac.2022.116549
13. W. Chen, L. Fan, M. Dong, L. Gao, X. Du, L. Wang, S. Su, L.-e Liu, Y. Wu, L. Ding, Emerging CRISPR/Cas-based strategies for extracellular vesicle detection: a comprehensive review. ACS Sens. **10**, 9135–9152 (2025). https://doi.org/10.1021/acssensors.5c02441
14. H. Yang, D.J. Patel, Structures, mechanisms and applications of RNA-centric CRISPR–Cas13. Nat. Chem. Biol. **20**, 673–688 (2024). https://doi.org/10.1038/s41589-024-01593-6
15. H. de Puig, R.A. Lee, D. Najjar, X. Tan, L.R. Soenksen, N.M. Angenent-Mari, N.M. Donghia, N.E. Weckman, A. Ory, C.F. Ng, P.Q. Nguyen, A.S. Mao, T.C. Ferrante, G. Lansberry, H. Sallum, J. Niemi, J.J. Collins, Minimally instrumented SHERLOCK (miSHERLOCK) for CRISPR-based point-of-care diagnosis of SARS-CoV-2 and

emerging variants. Sci. Adv. **7**, eabh2944 (2021). https://doi.org/10.1126/sciadv.abh2944
16. M.M. Kaminski, O.O. Abudayyeh, J.S. Gootenberg, F. Zhang, J.J. Collins, CRISPR-based diagnostics. Nat. Biomed. Eng. **5**, 643–656 (2021). https://doi.org/10.1038/s41551-021-00760-7
17. M. Duan, G. Li, J. Shen, R. Dai, X. Li, Z. Liu, F. Jia, A CRISPR/Cas12a biosensor for portable and accessible detection of *Salmonella typhimurium* via multi-indicator pH millidisc colorimetry and smartphone imaging platform. Biosens. Bioelectron. **286**, 117611 (2025). https://doi.org/10.1016/j.bios.2025.117611
18. X. Yin, H. Yang, Y. Piao, Y. Zhu, Q. Zheng, M.R. Khan, Y. Zhang, R. Busquets, B. Hu, R. Deng, J. Cao, CRISPR-based colorimetric nucleic acid tests for visual readout of DNA barcode for food authenticity. J. Agric. Food Chem. **70**, 14052–14060 (2022). https://doi.org/10.1021/acs.jafc.2c05974
19. Y. Kang, J. Zhang, L. Zhao, H. Yan, Colorimetric miRNA detection based on self-primer-initiated CRISPR-Cas12a-assisted amplification. Biotechniques **74**, 172–178 (2023). https://doi.org/10.2144/btn-2023-0008
20. R.S. Li, H. Liu, B.B. Chen, H.Z. Zhang, C.Z. Huang, J. Wang, Stable gold nanoparticles as a novel peroxidase mimic for colorimetric detection of cysteine. Anal. Methods **8**, 2494–2501 (2016). https://doi.org/10.1039/C6AY00367B
21. X. Wang, Q. Yao, X. Tang, H. Zhong, P. Qiu, X. Wang, A highly selective and sensitive colorimetric detection of uric acid in human serum based on MoS_2-catalyzed oxidation TMB. Anal. Bioanal. Chem. **411**, 943–952 (2019). https://doi.org/10.1007/s00216-018-1524-6
22. F. Qu, T. Li, M. Yang, Colorimetric platform for visual detection of cancer biomarker based on intrinsic peroxidase activity of graphene oxide. Biosens. Bioelectron. **26**, 3927–3931 (2011). https://doi.org/10.1016/j.bios.2011.03.013
23. A. Bano, A. Dawood, Rida, F. Saira, A. Malik, M. Alkholief, H. Ahmad, M.A. Khan, Z. Ahmad, O. Bazighifan, Enhancing catalytic activity of gold nanoparticles in a standard redox reaction by investigating the impact of AuNPs size, temperature and reductant concentrations. Sci. Rep. **13**, 12359 (2023). https://doi.org/10.1038/s41598-023-38234-2
24. J.C. Yu, J.H. Zhang, M. Li, Y.Q. You, C.C. Zhang, CRISPR/Cas13a-triggered entropy-driven amplification for colorimetric and fluorescent dual-mode detection of microRNA. Anal. Biochem. **689**, 115499 (2024). https://doi.org/10.1016/j.ab.2024.115499
25. Z.L. Yao, Q.N. Li, Y.J. Li, H.R. Li, S.W. Yang, C.Y. Wang, J.Y. Shi, S.L. Wu, S.Q. Liu, G.M. Han, J. Wang, L.Y. Xing, Y. Zhao, D.M. Kong, Q.L. Cai, CRISPR/Cas12a-based fluorescence-colorimetric dual-mode strategy for sensitive detection of clear cell renal cell carcinoma biomarker miR-210-3p. Sens. Actuators B Chem. **440**, 137923 (2025). https://doi.org/10.1016/j.snb.2025.137923
26. B. Luo, J. Zhou, X. Zhan, B. Ying, F. Lan, Y. Wu, Visual and colorimetric detection of microRNA in clinical samples based on strand displacement amplification and nanozyme-mediated CRISPR-Cas12a system. Talanta **277**, 126310 (2024). https://doi.org/10.1016/j.talanta.2024.126310
27. M.Y. Wang, S.X. Cai, Y.Q. Wu, Q. Li, X.L. Wang, Y.T. Zhang, N.D. Zhou, A lateral flow assay for miRNA-21 based on CRISPR/Cas13a and MnO_2 nanosheets-mediated recognition and signal amplification. Anal. Bioanal. Chem. **416**, 3401–3413 (2024). https://doi.org/10.1007/s00216-024-05290-0
28. X. Guo, T. Tian, X.C. Deng, Y. Song, X.M. Zhou, E.Q. Song, CRISPR/Cas13a assisted amplification of magnetic relaxation switching sensing for accurate detection of miRNA-21 in human serum. Anal. Chim. Acta **1209**, 339853 (2022). https://doi.org/10.1016/j.aca.2022.339853
29. S.F. Li, F.F. Wang, L. Hao, P.B. Zhang, G.Y. Song, Y.W. Zhang, C. Wang, Z. Wang, Q.H. Wu, Enhancing peroxidase activity of $NiCo_2O_4$ nanoenzyme by Mn doping for catalysis of CRISPR/Cas13a-mediated non-coding RNA detection. Int. J. Biol. Macromol. **283**, 137594 (2024). https://doi.org/10.1016/j.ijbiomac.2024.137594
30. X. Yang, Y. Luo, C. Su, Z. Huang, Y. Tang, L. Zhang, Ultra-sensitive biosensor detection of microRNA based on the CRISPR/Cas12a system and exonuclease-assisted target recycling signal amplification. Anal. Sci. **41**, 867–876 (2025). https://doi.org/10.1007/s44211-025-00755-3
31. S. Gong, X. Wang, P. Zhou, W. Pan, N. Li, B. Tang, AND logic-gate-based CRISPR/Cas12a biosensing platform for the sensitive colorimetric detection of dual miRNAs. Anal. Chem. **94**, 15839–15846 (2022). https://doi.org/10.1021/acs.analchem.2c03666
32. N. Yan, Z. Hu, L. Zhang, CRISPR-Cas13a-triggered DNAzyme signal amplification-based colorimetric miRNA detection method and its application in evaluating the anxiety. Appl. Biochem. Biotechnol. **196**, 7896–7907 (2024). https://doi.org/10.1007/s12010-024-04951-1
33. Y. Li, Q. Wang, Y. Wang, Direct and accurate miRNA detection based on CRISPR/Cas13a-triggered exonuclease-III-assisted colorimetric assay. J. Anal. Sci. Technol. **15**, 21 (2024). https://doi.org/10.1186/s40543-024-00434-4
34. Y. Yang, Y. Yang, X. Mao, W. Zhou, X.-F. Yu, G. Mao, Y. Ma, Multiplex microRNA detection for breast cancer precise diagnosis by constructing split crRNA-based amplification-free CRISPR/Cas12a biosensor. Chem. Eng. J. **522**, 167489 (2025). https://doi.org/10.1016/j.cej.2025.167489
35. M.-J. Lee, J.-H. Shin, S.-H. Jung, J.-W. Choi, H.R. Ahn, J.-H. Choi, B.-K. Oh, Hourglass-inspired total analysis system for the sensitive colorimetric detection of exosomal miRNA using the CRISPR-Cas12a system with isothermal amplification. Chem. Eng. J. **512**, 162729 (2025). https://doi.org/10.1016/j.cej.2025.162729
36. M.-J. Lee, J.-H. Shin, S.-H. Jung, H.R. Ahn, Y.J. Kim, J.-W. Choi, J.-H. Choi, B.-K. Oh, Single-tube total analysis system for ratiometric detection of exosomal miRNAs in breast cancer diagnosis. Chem. Eng. J. **529**, 173140 (2026). https://doi.org/10.1016/j.cej.2026.173140

Publisher's note

Springer Nature remains neutral with regard to jurisdictional claims in published maps and institutional affiliations.